

1 **First HFC-134a retrievals from ground-based FTIR solar**
2 **absorption spectra, comparison with TOMCAT model**
3 **simulations, *in-situ* AGAGE observations, and ACE-FTS**
4 **satellite data for the Jungfraujoch station**

5
6 Irene Pardo Cantos¹, Emmanuel Mahieu¹, Martyn P. Chipperfield^{2,3}, Christian
7 Servais⁴, Stefan Reimann⁵, and Martin K. Vollmer⁵

8 ¹Department of Astrophysics, Geophysics, and Oceanography, UR SPHERES, University of Liège, Liège, Belgium.
9 Corresponding author.

10 E-mail: i.pardocantos@uliege.be

11 Postal address: Allée du Six Août, 19, 4000 Liège, Belgium

12 ²School of Earth and Environment, University of Leeds, Leeds, UK

13 ³National Centre for Earth Observation, University of Leeds, Leeds, UK

14 ⁴Department of Astrophysics, Geophysics, and Oceanography, UR STAR, University of Liège, Liège, Belgium

15 ⁵Laboratory for Air Pollution and Environmental Technology, Empa, Swiss Federal Laboratories for Materials
16 Science and Technology, Switzerland

17
18
19
20 **ABSTRACT**

21 Successive regulations on the production and consumption of chlorofluorocarbons
22 (CFCs) and hydrochlorofluorocarbons (HCFCs) have led to the use of hydrofluorocarbons
23 (HFCs) as substitution products. Consequently, these potent greenhouse gases are now
24 controlled under the Kigali Amendment (2016) to the Montreal Protocol. HFC-134a is the
25 preferred substitute to CFC-12 as a refrigerant and is the most abundant HFC in the
26 atmosphere today. This work presents the first retrievals from ground-based Fourier
27 Transform InfraRed (FTIR) high-resolution solar absorption spectra, recorded at the
28 Jungfraujoch station as part of the Network for the Detection of Atmospheric Composition
29 Change (NDACC). To verify these retrievals, the FTIR time series was compared to three
30 other datasets: a simulation of the TOMCAT 3-D chemical transport model, the Fourier
31 Transform Spectrometer on board the Atmospheric Chemistry Experiment (ACE-FTS) L2 v5.2
32 retrievals, and the Jungfraujoch *in-situ* surface observations conducted within the Advanced
33 Global Atmospheric Gases Experiment (AGAGE) network. The overall trends of HFC-134a
34 (2004 – 2022) were analyzed to assess the relative growth rates of this atmospheric
35 compound. These trends are 7.34 ± 0.16 %/year (FTIR), 7.12 ± 0.05 %/year (TOMCAT), 7.29
36 ± 0.16 %/year (ACE-FTS), and 6.61 ± 0.05 %/year (*in-situ*). The relative trends are in good
37 agreement, so these novel FTIR retrievals are validated. Consequently, this strategy could be
38 implemented at other NDACC sites to achieve a quasi-global detection of this species using
39 the FTIR remote sensing technique.

40
41 **KEYWORDS**

42 HFC-134a, NDACC, TOMCAT/SLIMCAT, FTS, AGAGE, Trends

1. Introduction

Since the discovery of the implication of chlorofluorocarbons (CFCs) in stratospheric ozone depletion by Molina and Rowland (1974) [1], the Montreal Protocol on Substances that Deplete the Ozone Layer (1987) has aimed to limit the production and consumption of CFCs and other Ozone-Depleting Substances (ODSs) to protect the ozone layer and allow it to recover. The industry has therefore developed and produced substitutes for CFCs, the hydrochlorofluorocarbons (HCFCs). These substances have shorter atmospheric lifetimes and convey less chlorine atoms on a per molecule basis, which is why they are characterized by smaller ozone depletion potentials (ODPs). Still, HCFCs contribute to stratospheric ozone depletion, which led to their ban. Consequently, hydrofluorocarbons (HFCs), which are chlorine- and bromine-free molecules that do not affect the ozone layer, have been introduced to replace both CFCs and HCFCs [2]. Nevertheless, all these substances are strong infrared (IR) radiation absorbers and hence contribute to the Earth's radiative forcing [3]. As HFCs are very potent greenhouse gases, they were included in the list of substances controlled by the Kyoto Protocol (1997), but no emission limits were established. Therefore, the Kigali Amendment (2016) to the Montreal Protocol came into force in 2019 to gradually reduce the global production and use of long-lived HFCs [4]. HFCs are mainly used in refrigeration systems, air conditioning, and foam-blowing as well as firefighting agents and propellants [4]. In the last years, the consumption and emissions of CFCs have decreased. While HCFC consumption and emissions have stabilized in recent years, those of the HFCs continue to rise [4]. Since 2000, global HFC emissions estimated from atmospheric observations show a significant gap to the total CO₂-eq HFC emissions reported by Annex I countries to the United Nations Framework Convention on Climate Change (UNFCCC) in 2019 (Fig. 2-2 in [5]). Unfortunately, this gap between estimated and reported emissions has been broadening in the recent years. This difference could be explained by emissions from non-Annex I countries and/or by unrecorded emissions, considering that many countries still do not report to the UNFCCC or remain not monitored by atmospheric observations [4]. The total CO₂-equivalent emissions (based on 100-yr time horizon Global Warming Potential, GWP) by HFCs in 2020 has been estimated to be 1.22 ± 0.05 Gt CO₂-eq yr⁻¹ [4].

1,1,1,2-Tetrafluoroethane or CH₂FCF₃ (HFC-134a) has replaced CFC-12 as the preferred refrigerant and is the most abundant HFC in the atmosphere [4]. Its total atmospheric lifetime is 13.5 years (14.1 years in the troposphere and 313 years in the stratosphere) [6]. The large difference between the tropospheric and the stratospheric lifetimes is due to the reaction with tropospheric OH, the main atmospheric sink for HFC-134a (responsible for 99% of its atmospheric degradation) [2]. Atmospheric HFC-134a loss produces COF₂, HF and trifluoroacetic acid (TFA; CF₃COOH). This is a toxic breakdown product that accumulates in water reservoirs through wet deposition. However, it is known that the environmental impact of TFA still needs to be investigated [7]. It is estimated that HFC-134a emissions started in the early 1990s as the atmospheric HFC-134a levels began to rise in the mid-1990s. This is based on global *in-situ* measurements by NOAA (National Oceanic and Atmospheric Administration) [8; 9]. The GWP of HFC-134a is 1470 (100-yr) and it is the largest contributor to radiative forcing from HFCs with 44% of their total contribution (44.1 ± 0.6 mW m⁻²) in 2020, which is about 30% more than in 2016. The share of HFC-134a in total HFCs emissions in 2020 is about 30%, which is an increase of about 20% since

1 2016 [4]. Global emissions of HFC-134a estimated by the Advanced Global
2 Atmospheric Gases Experiment (AGAGE) and NOAA networks are, $247 \pm 28 \text{ Gg yr}^{-1}$
3 (or $364 \pm 41 \text{ Tg CO}_2\text{-eq yr}^{-1}$) and $243 \pm 27 \text{ Gg yr}^{-1}$ (or $358 \pm 39 \text{ Tg CO}_2\text{-eq yr}^{-1}$),
4 respectively in 2020 [4].

5 In this work, we describe the first retrieval strategy from ground-based Fourier
6 Transform InfraRed (FTIR) solar absorption spectra, and we analyze the HFC-134a
7 atmospheric abundances above the Jungfraujoch station. To evaluate this first HFC-
8 134a FTIR time series, we compare our retrieved total columns (presented as dry air
9 mole fractions) to surface air measurements (AGAGE), satellite data (ACE-FTS
10 instrument on board SCISAT) over Europe and TOMCAT model simulations for the
11 period from January 2004 to December 2022. In Section 2, we describe the FTIR, *in-*
12 *situ* and satellite observations as well as the 3-D chemical transport model. In Section
13 3, we describe the retrieval strategy, and in Section 4, we present the results and
14 discuss the trend analysis for the different datasets. Finally, we conclude this study in
15 the section “Summary and conclusions”.

17 **2. Measurement methods and datasets**

18 **2.1 NDACC FTIR observations at the Jungfraujoch station**

19
20 The FTIR spectra used in this study were recorded under clear-sky conditions
21 at the Jungfraujoch research station (46.55°N , 7.98°E) in the Swiss Alps at 3580 m
22 above mean sea level (a.m.s.l.). The Jungfraujoch station is located between the
23 Mönch (4107 m) and the Jungfrau (4158 m) summits, in a very dry area compared to
24 other NDACC stations, due to the high altitude and the proximity of the Aletsch glacier
25 [10]. Spectra have been recorded since the early 1950s by the team of the Institute of
26 Astrophysics of the University of Liège (Belgium). The high-resolution FTIR
27 measurements began in 1984 [11] and are now conducted as part of the Network for
28 the Detection of Atmospheric Composition Change (NDACC) [12]. The retrievals
29 presented in this article were obtained from a subset of high-resolution infrared (IR)
30 solar absorption spectra recorded with a Bruker IFS-120HR spectrometer, modified by
31 the team, and in operation since the early 1990s. These observations were made with
32 a HgCdTe (mercury cadmium telluride, MCT) detector and they cover the $700 - 1400$
33 cm^{-1} spectral range with a spectral resolution of 0.0061 cm^{-1} , that is a maximum optical
34 path difference (OPD) of 82 cm.

35 **2.2 AGAGE *in-situ* observations at the Jungfraujoch station**

36
37 In addition to measurements by FTIR, fully independent observations of HFC-
38 134a at Jungfraujoch are also available through *in-situ* measurements using
39 preconcentration gaschromatography – mass spectrometry (GCMS) [13]. As part of a
40 suite of ~50 halogenated substances, high-precision HFC-134a measurements have
41 been conducted within the AGAGE network [14]. At Jungfraujoch, measurements
42 began in 2000 using a GCMS-ADS (adsorption/desorption) system [15] followed by
43 Medusa-GCMS technology in 2008 [14; 16]. For the Medusa-GCMS, 2 L samples are
44 preconcentrated on a first trap and held at $\sim -160^\circ\text{C}$. The samples are desorbed at

1 100°C and cryofocussed on a second trap before injection into the GCMS. The
2 measurement of one sample takes about 70 minutes. After each pair of air samples,
3 a calibration gas (quaternary standard) is measured to track and correct for MS signal
4 drift. Measurement precision for HFC-134a is about 0.3% (1- σ). The HFC-134a
5 measurements are fully intercalibrated within the AGAGE network and are reported as
6 dry-air mole fraction in pmol mol⁻¹ (parts-per-trillion, ppt) on the Scripps Institution of
7 Oceanography (SIO) calibration scale SIO-05 with an estimate accuracy of ~2%. For
8 the present study, only baseline measurements (deemed representative for a broad
9 atmospheric region) were used, based on a statistical filtering algorithm [17; 18].

10 11 **2.3 ACE-FTS observations**

12 The ACE-FTS instrument on board the Atmospheric Chemistry Experiment
13 (ACE), also known as SCISAT, is the main instrument of this Canadian satellite [19].
14 SCISAT was launched into low Earth circular orbit by NASA in August 2003. Since
15 February 2004, this satellite has been collecting data of the atmospheric pressure,
16 temperature, and several molecular abundances [20]. ACE-FTS is a Fourier
17 Transform Spectrometer (FTS) that records up to 30 IR transmittance spectra per day
18 at sunrise and sunset by solar occultation. The locations of the occultations are
19 determined by the orbit of the satellite and its relative position to the Sun [2]. This
20 instrument operates in the range from 750 to 4400 cm⁻¹ with a spectral resolution of
21 0.02 cm⁻¹ [20]. The signal-to-noise ratio (SNR) ranges from about 100:1 to about 400:1
22 [21]. The vertical resolution averages about 3 km and each occultation analyzes the
23 atmosphere from 150 km down to the cloud tops, or down to 5 km at best under clear-
24 sky conditions [2]. Five micro-windows (MW) are used for the HFC-134a retrievals:
25 MW₁ = 828.78 – 829.28 cm⁻¹; MW₂ = 1090.20 – 1090.60 cm⁻¹; MW₃ = 1103.04 –
26 1105.84 cm⁻¹; MW₄ = 1949.93 – 1950.28 cm⁻¹; and MW₅ = 2623.63 – 2624.28 cm⁻¹
27 [20]. For this study, we used ACE-FTS Level 2 v5.2 retrievals of the HFC-134a
28 molecular abundances, expressed as volume mixing ratios (VMRs), from 5.5 km to
29 15.5 km for a latitude band around the Jungfrauoch station (40-50°N). We limited the
30 ACE-FTS measurements to 15.5 km because the vertical profile decreases
31 meaningfully above this altitude [19; 2]. Further information on the ACE-FTS version
32 5 retrievals can be found in Boone et al. (2023) [21].

33 34 **2.4 The TOMCAT/SLIMCAT chemical transport model**

35 To help interpret the observations, we used output from a simulation of the
36 TOMCAT/SLIMCAT (hereafter TOMCAT) three-dimensional (3-D) chemical transport
37 model (CTM) [22]. The simulation used here had a horizontal resolution of 2.8° × 2.8°
38 with 32 levels from the surface to ~ 60 km. The model was forced using meteorology
39 from European Centre for Medium-Range Weather Forecasts (ECMWF) ERA5
40 reanalyses [23] and was integrated from 1979 until 2022. The model contained a
41 detailed treatment of stratospheric chemistry including interactive calculation of
42 photochemistry (OH, photolysis) relevant for HFCs.

43 The model run was constrained by specifying the monthly mean global mean
44 surface VMRs of the long-lived source gases. For species such as CFCs and HCFCs

1 these are taken from the Scientific Assessment of Ozone Depletion (2018) [24]. For
2 HFCs, including HFC-134a, the global mean surface VMRs are taken from the NOAA
3 Annual Greenhouse Gas Index (data obtained from
4 <https://gml.noaa.gov/aggi/aggi.html>). This boundary condition constraint means that
5 the model does not simulate the spatial and short-term temporal variation in the
6 surface concentration of HFC-134a. The model does, however, simulate the relative
7 HFC-134a profile shape through atmospheric transport and loss processes. For
8 comparison with observations the simulated model profile was sampled daily (at 0 UT)
9 at the location of Jungfraujoch.

11 **3. HFC-134a total column retrievals**

12 **3.1 Retrieval strategy**

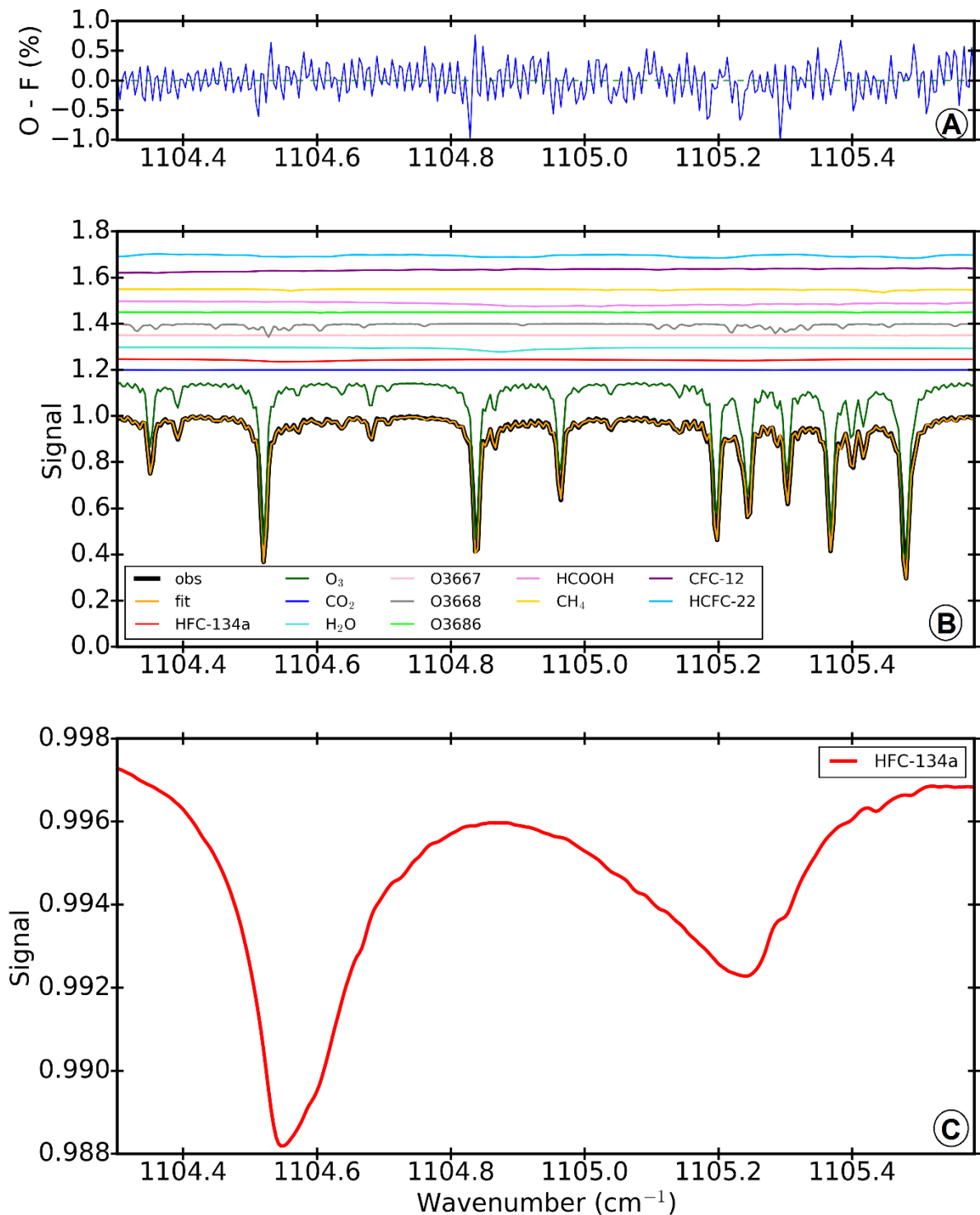
14 Since the main absorber in the infrared domain is water vapor, the dry
15 conditions of the Jungfraujoch station facilitate the detection, retrieval, and analysis of
16 trace gases with very weak spectral absorptions, such as HFC-134a. The application
17 to other NDACC sites has yet to be tested.

18 We investigated all the significant HFC-134a features included in the pseudo-
19 line list produced by G. C. Toon from the Jet Propulsion Laboratory
20 (<https://mark4sun.jpl.nasa.gov/>), which is based on six laboratory absorption cross-
21 section datasets from Clerbaux et al. (1993) [25]; Highwood and Shine (2000) [26];
22 Nemtchinov and Varanasi (2004) [27]; Sharpe et al. (2004) [28]; Gohar et al. (2004)
23 [29]; and Harrison (2015) [30] ([https://mark4sun.jpl.nasa.gov/data/spec/Pseudo/HFC-
24 134a_PLL.compressed.pdf](https://mark4sun.jpl.nasa.gov/data/spec/Pseudo/HFC-134a_PLL.compressed.pdf)). However, only two were suited for the inversion of our
25 ground-based solar atmospheric spectra: $1104.300 - 1105.585 \text{ cm}^{-1}$ and $1182.0 -$
26 1186.4 cm^{-1} . In this work, we will only present the results for the first window since the
27 second one shows a strong water vapor absorption between about 1185.0 cm^{-1} and
28 1186.4 cm^{-1} , which masks the main absorption of HFC-134a, even at Jungfraujoch. In
29 addition, the HFC-134a absorption in the second window is smaller and more
30 unstructured than in the first window. Please, consult Figure 1 in the supplementary
31 materials for more information about the second spectral window. The first window
32 range was also used by the ACE-FTS team for the HFC-134a retrievals [20]. To
33 maximize the absorption depth of our target molecule and the information content,
34 only the subset of observations with an apparent solar zenith angle (SZA) between
35 60° and 85° was fitted. For this work, we did not filter the observations according to
36 water vapor or ozone columns since there is no dependency to the air mass, or the
37 H_2O or O_3 total columns (Figure 2 in the supplementary materials). However, some
38 filtering could be necessary in more humid sites or in sites located at lower altitudes
39 than Jungfraujoch.

40 For the retrieval of the HFC-134a total columns, we adopted a Tikhonov L1
41 regularization with an α -parameter of 50. The simulations and retrievals of the total
42 columns were performed using the SFIT-4 v1.0.18 algorithm, which applies the
43 Optimal Estimation Method (OEM) of Rodgers, 2000 [31]. The layer scheme spanned

1 41 layers from 3.58 km to 120 km high, and thickness gradually rose from 0.65 km for
2 the lowest layer up to 14 km for the highest layer.

3



4

5 **Figure 1.** Spectral window for HFC-134a. Panel A displays the observed – calculated
6 residuals, in %, from the simulation to the spectrum recorded on May 25, 2016. The root-
7 mean-square of the fitting residuals is 0.27%. Panel B shows the simulation of the 1104.300
8 – 1105.585 cm^{-1} spectral window for spectra recorded by the Bruker IFS-120HR FTIR
9 instrument at the Jungfraujoch station at an apparent solar zenith angle of 77.2°, and a

1 maximum optical path difference of 82 cm. The signal-to-noise ratio for this spectrum is 952.
2 The main interfering species (O_3 , CO_2 , H_2O , the ozone isotopologues, $HCOOH$, CH_4 , CFC-12,
3 and HCFC-22) are shifted vertically for clarity. Be aware of the scale of the vertical axis in
4 Panel C, where the HFC-134a absorption is magnified.

5 The simulated interfering species are CO_2 , H_2O , O_3 , some ozone isotopologues
6 ($O3667$, $O3668$, and $O3686$), formic acid ($HCOOH$), CH_4 , CCl_2F_2 (CFC-12), and
7 $CHClF_2$ (HCFC-22). These interfering molecules were also used for the HFC-134a
8 ACE-FTS retrievals by Fernando et al. (2019) [20]. The spectroscopic parameters for
9 the interfering species were obtained from the HITRAN2020 database [32] and the
10 empirical pseudo-line list created by G. C. Toon for the unresolved features of the
11 halocarbons (<https://mark4sun.jpl.nasa.gov/pseudo.html>). The spectroscopic
12 parameters of water vapor were obtained from the ATM20
13 (<https://mark4sun.jpl.nasa.gov/specdata.html>) compilation.

14 *A priori* profiles of the interfering species were obtained from the Whole
15 Atmosphere Community Climate Model (WACCM, version 6; [33]) climatological
16 profiles over the period 1980 – 2040, except for water vapor. *A priori* profiles of water
17 vapor were supplied by the ERA-Interim [34] and ERA-5 [23] meteorological
18 reanalyzes complemented with WACCMv6 monthly means for the uppermost
19 atmospheric layers. Since HFC-134a is not included in the WACCM simulations, we
20 used the ACE-FTS vertical distribution for 2006 [2] as a *a priori* profile for HFC-134a for
21 the upper troposphere and lower stratosphere (5 – 15 km). The lower tropospheric *a*
22 *priori* profile was considered constant from the lower limit of ACE-FTS HFC-134a
23 profile (5 km). In the same way, the middle stratospheric *a priori* profile was considered
24 constant from the upper limit of ACE-FTS HFC-134a profile (15 km). Using another
25 year profile, for example 2018 [2], as a *a priori* has no measurable effect on the retrieved
26 FTIR products.

27 Panel B in Figure 1 shows a simulation of the $1104.300 - 1105.585 \text{ cm}^{-1}$
28 spectral window. The observed spectrum (obs) is displayed in black and the simulated
29 spectrum (fit) is shown in orange. Each individual molecule is shown in the colors
30 indicated in the legend. As can be observed, the main interferences in this window are
31 due to ozone (in dark green). The absorption feature of HFC-134a (in red, Panel C)
32 peaks around 1104.55 cm^{-1} and 1105.24 cm^{-1} , surrounding the water vapor absorption
33 (in light turquoise) in the center of the window. Even though the interferences from the
34 other molecules appear very weak, we cannot ignore them since the absorption of our
35 target molecule represents only about 1% (Panel C), so any small contribution from
36 other species can be important for the retrievals. Panel A shows the fitting residuals
37 (observed – calculated) from the simulated spectrum to a spectrum obtained on May
38 25, 2016. The residuals are close to the noise level, except around some of the most
39 intense ozone absorption lines. The root-mean-square (RMS) of the fitting residuals is
40 0.27% and the H_2O total column is $7.3 \times 10^{21} \text{ molec. cm}^{-2}$ for this example. This
41 spectrum is a good representation of the whole time series (2004 – 2022), as the
42 median and mean RMS are 0.27% and 0.28%, respectively, and the median and the
43 mean H_2O total columns are $5.4 \times 10^{21} \text{ molec. cm}^{-2}$ and $6.8 \times 10^{21} \text{ molec. cm}^{-2}$,
44 respectively. This spectrum was recorded with a maximum OPD of 82 cm at a solar

1 zenith angle of 77.2°, which is at the median of the SZA of the whole spectra used in
 2 this study.

3

4 **3.2 Uncertainty analysis of the measurements**

5 The main sources of error affecting the retrievals of the total columns are listed
 6 in Table 1. This uncertainty budget was calculated for one year of spectra (2014),
 7 taken as an example in the middle of the time series. The random and systematic
 8 components are presented separately. To create the random component of the error
 9 covariance matrix, we used a constant relative standard deviation of 18%, based on
 10 ACE-FTS L2 v5.2 HFC-134a retrievals [21], for each level of the grid (1 km-levels
 11 between 5.5 and 15.5 km; between 40 and 50°N) which represents the average
 12 relative standard deviation for four months of the ACE-FTS time series (April – July
 13 2012). The systematic part was produced using the mean relative difference between
 14 the ACE-FTS L2 v5.2 HFC-134a retrievals and the TOMCAT simulations in the lowest
 15 model layer for the same four months. The model simulations were used for this
 16 estimation as no other satellite observations are currently available. A constant relative
 17 difference of 10% was used for each layer of the grid. This value is similar to the
 18 systematic component used for HCFC-22 by Prignon et al. (2019) [35]. The correlation
 19 width of the HFC-134a profile was assumed to be 3 km. The random uncertainty for
 20 the SZA was set to $\pm 0.1^\circ$, while the systematic uncertainty was assumed to be $\pm 0.03^\circ$.
 21 The relative systematic uncertainties of the spectroscopic parameters of HFC-134a
 22 (line intensity, temperature, and pressure) were set to 5%, according to the empirical
 23 pseudo-line list produced by G. C. Toon.

24

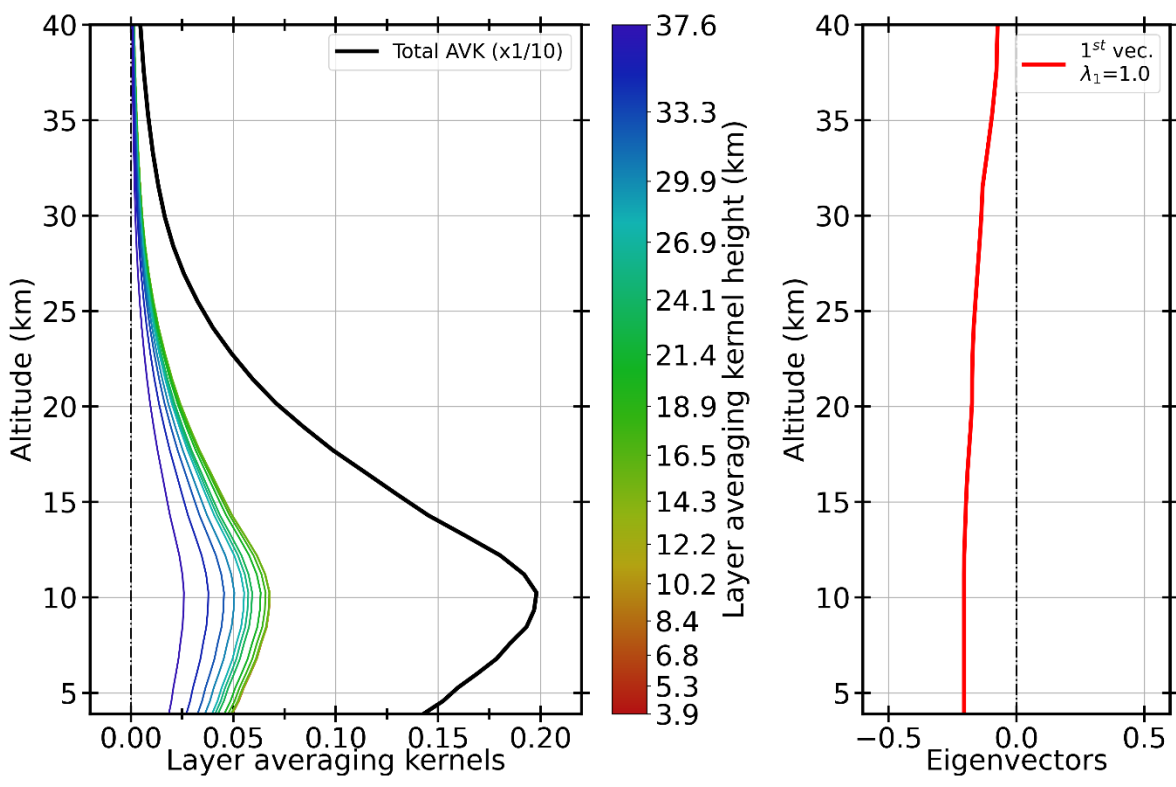
25 **Table 1.** Mean relative uncertainties (%) for one year (2014) concerning the HFC-134a total
 26 column retrievals for the Jungfaujoch station.

Error type and source	Relative uncertainty (%)	
	Mean	Standard deviation
Random components		
Measurement	6.7	2.2
Temperature	4.3	1.0
SZA	0.8	0.3
Interfering species	5.5	1.9
Smoothing	1.0	0.1
Retrieval parameters	0.3	0.2
Total random	9.8	2.8
Systematic components		
HFC-134a line intensity	4.99	0.01
Temperature	7.1	1.9
SZA	0.3	0.1
Total systematic	8.9	1.5

27

1 The mean total random and systematic uncertainties are $9.8 \pm 2.8 \%$ and $8.9 \pm$
 2 1.5% , respectively. The error budgets for 5 years before and after 2014 were also
 3 calculated. For 2009, the total random and systematic uncertainties are $14.5 \pm 3.8 \%$
 4 and $13.3 \pm 3.0 \%$, respectively, while for 2019, they are $8.5 \pm 2.5 \%$ and $7.1 \pm 1.1 \%$,
 5 respectively. These results highlight the challenge to retrieve HFC-134a from ground-
 6 based FTIR solar absorption spectra in the early 2000s, while the atmospheric load
 7 only started to develop in the mid-1990s. Consequently, we decided to show here the
 8 HFC-134a total columns above Jungfraujoch from 2004 to 2022, spanning the same
 9 period as the ACE dataset. As shown in Table 1, the random error is mainly
 10 determined by the uncertainties of the measurement, the temperature, and the
 11 interfering species, while the systematic error is mainly influenced by the uncertainty
 12 of the spectroscopic parameters. The other sources of uncertainty only contribute less
 13 than 1% to the total error (random and systematic). These relative uncertainties are
 14 determined by dividing the measurement uncertainty by the absolute total column
 15 value.

16



17
 18 **Figure 2.** Mean layer averaging kernels and first eigenvector. The left panel shows the mean
 19 layer averaging kernels for mixing ratios computed for the spectra recorded at the
 20 Jungfraujoch station from January 2007 to December 2009. The ticks on the color bar are the
 21 individual layer averaging kernels represented in the graph. The first eigenvector is shown in
 22 the right panel and its eigenvalue is 1.0.

23
 24 The mean layer averaging kernels provide the information content of the
 25 retrieval processing required to characterize the relative weighting between the *a priori*
 26 and the true vertical profiles to the retrieved vertical distribution [31]. Figure 2 shows

1 the mean layer averaging kernels (left panel) and the first eigenvector (right panel)
2 calculated for the spectra recorded above the Jungfraujoch station in 3 years (2007 –
3 2009). The thick black line indicates the total column averaging kernel scaled by 0.1
4 (from 3.58 km, the station altitude, up to 40 km), while the colored lines show the
5 different individual layer averaging kernels, indicated by the vertical color bar. The
6 degrees of freedom for signal (DOFS) inform on how much information can be
7 extracted from the retrievals. The mean DOFS of the entire time series is 1.0, so the
8 retrievals provide one useful piece of information. The 100% of the information
9 characterizing the troposphere comes from the retrievals and not from the assumed *a*
10 *priori*, as indicated by the first eigenvalue ($\lambda_1 = 1.0$).

11 We also analyzed the effects of the misalignment of the Bruker 120HR
12 spectrometer between July 2011 and December 2012, because the retrieved total
13 columns presented a discontinuity in this period, with a local maximum that was not
14 observed in the other datasets. For this purpose, we retrieved an effective apodization.
15 Nevertheless, this perturbation did not show consistent effects on the retrieved total
16 columns. This effect was also observed in the partial columns of other species
17 retrieved at the Jungfraujoch station during the same period, such as HCFC-22 [35].

18

19 **4. Results and discussion**

20 In this section, we present the HFC-134a time series obtained after the retrieval
21 of the total columns, as well as the trend analyzes and seasonality. Since these are
22 the first HFC-134a retrievals from ground-based FTIR solar absorption spectra, we
23 compare our results with other three independent datasets, described in Section 2.

24

25 **4.1 Time series of HFC-134a above the Jungfraujoch NDACC site**

26 With the aim of keeping good spectra, we did not consider data with a fit RMS
27 higher than 0.6 (considering that the mean fit RMS is 0.3). We also removed data from
28 July 2011 to December 2012 due to the low reliability of the retrievals, as explained in
29 the section above. Before filtering, we had 5019 spectra for the whole time series
30 (January 2004 – December 2022), i.e. 1542 daily measurements. After filtering, we
31 retained specifically 1382 daily observations (196 months). To use the same units and
32 to easily compare the four independent time series, we show here the FTIR dry air
33 mole fractions (xHFC-134a) instead of the retrieved total columns. These xHFC-134a
34 were determined by dividing the HFC-134a total columns by the dry air pressure
35 column (DPC), which can be obtained as described in Barthlott et al. (2015) [36], and
36 Pardo Cantos et al. (2022) [37]. The water vapor columns used to calculate the xHFC-
37 134a were obtained using a dedicated retrieval strategy for water vapor, described by
38 Sussmann et al. (2009) [38].

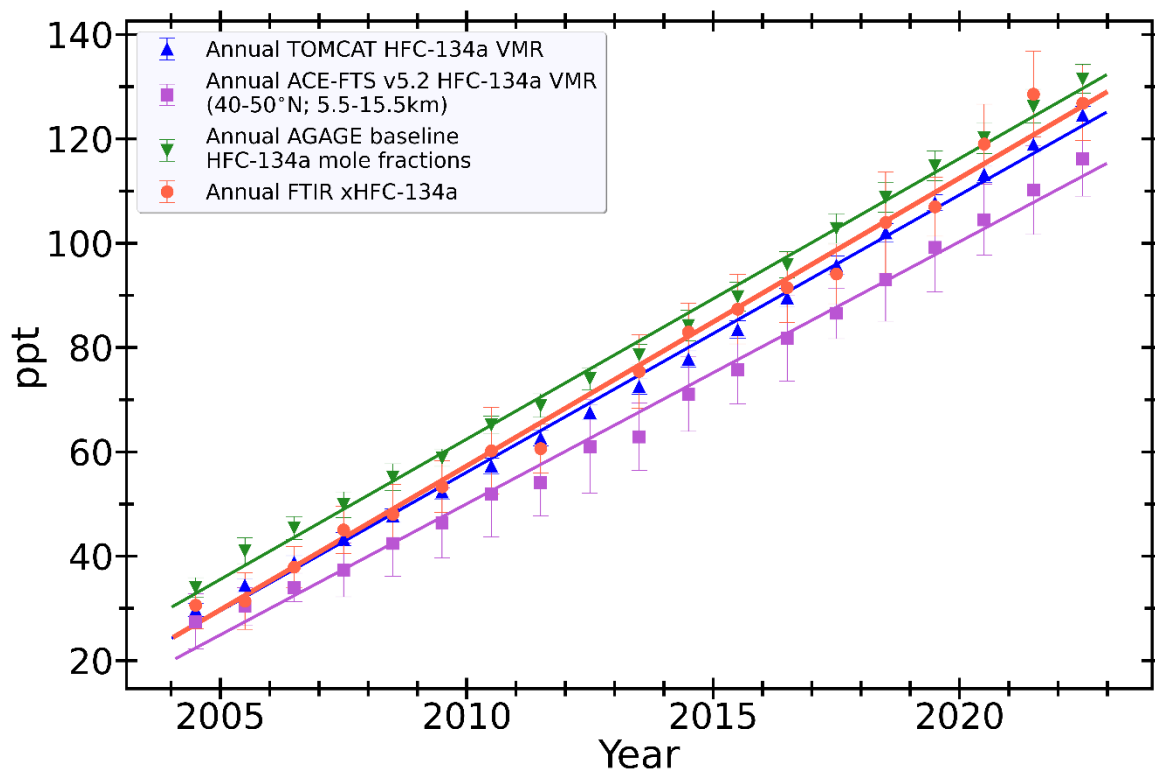
39

40 **4.2 Comparisons with independent datasets**

41 Figure 3 shows the annual means of the four different datasets from January
42 2004 to December 2022. As orange dots, the xHFC-134a from FTIR measurements

1 at the Jungfraujoch station; in blue up-pointing triangles, the HFC-134a surface
 2 volume mixing ratios derived from TOMCAT model simulations; in purple squares , the
 3 HFC-134a VMRs from ACE-FTS for a latitude band between 40 and 50°N (centered
 4 around the Jungfraujoch station location) and averaged over an altitude range
 5 between 5.5 and 15.5 km; finally, the green down-pointing triangles show the *in-situ*
 6 HFC-134a mole fractions measured at the Jungfraujoch station within the AGAGE
 7 network. The error bars show the standard deviation around the annual means. The
 8 mean relative standard deviations are 9.5% for the FTIR annual xHFC-134a averages,
 9 commensurate with the random uncertainty shown in Table 1; 2.3% for the annual
 10 means of the TOMCAT model surface VMRs; 10.9% for the ACE-FTS HFC-134a
 11 VMRs; and 3.4% for the *in-situ* baseline mole fractions.

12



13

14 **Figure 3.** Atmospheric HFC-134a annual means derived from the different datasets. As
 15 orange dots, the Jungfraujoch FTIR xHFC-134a data; as blue up-pointing triangles, the
 16 TOMCAT HFC-134a lower-most model level VMRs; as purple squares, the ACE-FTS L2 v5.2
 17 HFC-134a VMRs; and as green down-pointing triangles, the *in-situ* baseline HFC-134a mole
 18 fractions at Jungfraujoch. The vertical error bars depict one standard deviation. The respective
 19 linear trends are indicated by the straight lines.

20

21 For the FTIR time series, some periods must be emphasized. First, the 2021
 22 annual mean is higher because the spectrometer was out of operation from January
 23 to May 2021, so this annual mean only includes the second half of the year, when the
 24 atmospheric HFC-134a content is higher, as shown in Figure 4. In addition, the quality
 25 of the spectra from 2021 is less accurate as the maintenance of the Bruker 120HR
 26 spectrometer could not be performed frequently enough due to travel restrictions. The
 27 second period to note extends from July 2011 to December 2012. This one-and-a-

1 half-year data was suppressed because of the low quality of the retrievals during this
 2 period, as explained in Section 3. Consequently, the 2011 xHFC-134a annual mean
 3 is slightly lower because we only considered the first half of the year, when the
 4 atmospheric HFC-134a burden is lower.

5 The FTIR and TOMCAT model time series are in good quantitative agreement.
 6 In fact, the mean relative systematic difference between TOMCAT VMRs and FTIR
 7 xHFC-134a monthly means is 5.3%, which is covered by the systematic uncertainty of
 8 the retrievals shown in Table 1. This mean relative systematic difference between the
 9 two datasets was determined by dividing the difference of the mean TOMCAT and
 10 FTIR values by the mean TOMCAT VMR. While the two datasets almost overlap for
 11 the earlier years, they diverge slightly later on. Still, the respective trends are
 12 consistent when the associated statistical uncertainties are considered. The ACE-FTS
 13 time series seems to be down shifted compared to the FTIR series, while the *in-situ*
 14 baseline HFC-134a time series is higher than the FTIR time series. However, we
 15 should not forget that the ACE-FTS observations mainly represent the upper
 16 troposphere, as only a subset of the measured profiles reached down to 5.5 km. While
 17 the *in-situ* measurements are representative of the surface mole fractions, the FTIR
 18 observations are less sensitive in the first few kilometers of the atmosphere, and they
 19 reach a maximum around 10 km to then decrease rapidly above, as shown in Figure
 20 2. The differences between the four datasets may have several causes including the
 21 time required for vertical transport and mixing. The systematic uncertainty reported in
 22 Table 1 could also explain part of the bias between the *in-situ* and the remote sensing
 23 datasets.

24

25 **4.3 Trend analyses and seasonality**

26 We analyzed the linear trend of the entire FTIR time series (2004 – 2022). The
 27 trends and their uncertainties were estimated using the autoregressive wild bootstrap
 28 method developed by Friedrich et al. (2020) [39] with a 95% confidence interval. The
 29 absolute and relative linear trends are gathered in Table 2. These trends were
 30 calculated using the monthly means, even if only the annual means are shown in
 31 Figure 3 for reasons of clarity. The relative trends were calculated by dividing the
 32 absolute trend by the mean value (dry air mole fractions, or VMRs, or baseline mole
 33 fractions) of the whole time series.

34

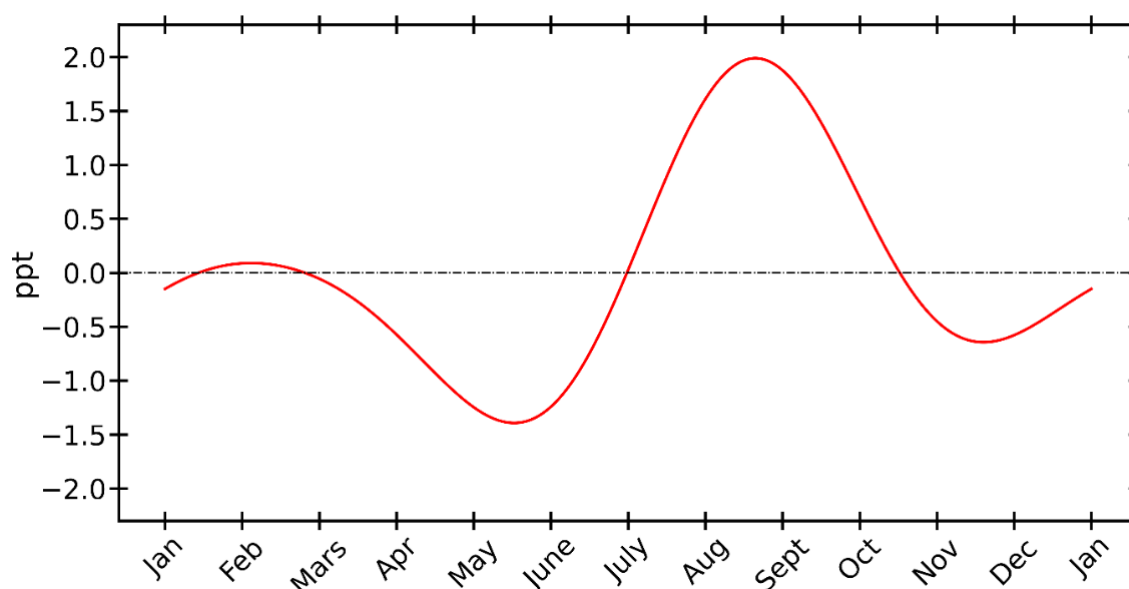
35 **Table 2.** Relative and absolute trends derived for the FTIR xHFC-134a at Jungfraujoch, the
 36 TOMCAT surface HFC-134a VMRs, the AGAGE HFC-134a mole fractions at Jungfraujoch,
 37 and the ACE-FTS HFC-134a VMRs, for the 2004 – 2022 period.

Source	Trend (ppt yr ⁻¹)	Relative trend (% yr ⁻¹)
xHFC-134a FTIR	5.52 ± 0.12	7.34 ± 0.16
TOMCAT surface VMR	5.32 ± 0.04	7.12 ± 0.05
ACE-FTS v5.2 HFC-134a VMR	5.02 ± 0.11	7.29 ± 0.16
AGAGE baseline mole fractions	5.38 ± 0.04	6.61 ± 0.05

38

1 We found that the HFC-134a atmospheric concentration according to the FTIR
2 measurements above the Jungfraujoch site increased by 5.52 ± 0.12 ppt per year, or
3 a relative increase of 7.34 ± 0.16 % per year. Regarding the other time series, a rise
4 of 7.12 ± 0.05 % per year (TOMCAT), 7.29 ± 0.16 % per year (ACE-FTS), and $6.61 \pm$
5 0.05 % per year (*in-situ*) was observed. Therefore, the FTIR, TOMCAT and ACE
6 relative trends agree when we weigh the uncertainties. The *in-situ* relative trend is
7 slightly lower by about 8%.

8 Other studies have already analyzed the atmospheric HFC-134a trends
9 (Montzka et al. (2015) [9], Fernando et al. (2019) [20], Harrison et al. (2021) [2]). The
10 Scientific Assessment of Ozone Depletion [4] reports an increase in global HFC-134a
11 from 85.5 ± 0.3 ppt in 2016 to 109.8 ± 0.2 ppt in 2020 in the upper troposphere. A
12 study by Bernath et al. (2021) [40] describes a global trend for the ACE-FTS Level 2
13 v4.1 HFC-134a retrievals (2004 – 2020) of 5.71 ± 0.07 ppt per year, that is 6.86 ± 0.22
14 % per year, which is in line with our results.



16
17 **Figure 4.** Seasonal cycle of xHFC-134a as derived from the FTIR observations at the
18 Jungfraujoch station. The minimum atmospheric HFC-134a is at the end of spring, while the
19 maximum occurs at the end of the summer.

20
21 Finally, we analyzed the seasonal cycle of xHFC-134a (Figure 4), which
22 exhibits minimum abundances at the end of spring (May-June), and maximum load at
23 the end of summer (August-September). A local minimum is present in November, and
24 a local maximum in February. It is important to note that the seasonal cycle peak-to-
25 peak amplitude is relatively weak, around 3.5 ppt, that is 4.5%. This behavior is also
26 captured by the TOMCAT seasonal cycle, where the maximum occurs in early
27 September and the minimum in early April. The annual cycle of the *in-situ* baseline
28 HFC-134a mole fractions at Jungfraujoch shows a minimum at the end of winter and
29 a maximum load during the spring and summer. These *in-situ* baseline measurements
30 can account for the regional emissions and their main sink is oxidation by the OH
31 radical. However, the FTIR measurements are also influenced by the tropopause

1 height and the atmospheric circulation. Above the Jungfraujoch site, the mean
2 tropopause height is around 11.3 ± 2.2 km (2- σ) [41, 42]. On the one hand, the
3 tropopause above Jungfraujoch sinks in fall and winter and reaches a minimum height
4 at the beginning of March. On the other hand, the tropopause above the station rises
5 in spring and summer and gets a maximum height in mid-August [41].

7 **Summary and conclusions**

8 In this study, we described the retrieval strategy we developed for HFC-134a
9 from ground-based FTIR solar absorption spectra recorded at the high-altitude dry
10 Jungfraujoch station. This was the first attempt to retrieve HFC-134a within the
11 NDACC network. HFC-134a is the most abundant HFC in the atmosphere and the
12 preferred substitute to CFC-12 as a refrigerant. Even though HFCs do not directly
13 affect stratospheric ozone, they are very potent greenhouse gases, which is why they
14 were included in the Kigali Amendment to the Montreal Protocol.

15 We chose the $1104.300 - 1105.585$ cm^{-1} spectral window for the retrievals, in
16 which the HFC-134a feature typically represents only 1% of the absorption depth. We
17 chose this window as the water vapor absorption is not very intense, which is an
18 essential point to consider in the cases where the absorption of the target molecule is
19 weak. The main interfering species in this window is ozone and its absorption lines are
20 well defined. The mean DOFS is equal to 1.0, which allows the determination of a
21 single piece of information.

22 The trend of xHFC-134a was analyzed from January 2004 to December 2022.
23 The previous years were not analyzed because the FTIR retrievals in early 2000 are
24 quite challenging for this molecule, as demonstrated in the error budget analysis
25 section. The obtained FTIR HFC-134a time series was compared to three other
26 independent datasets: TOMCAT model simulations, ACE-FTS satellite observations,
27 and AGAGE *in-situ* surface measurements also performed at the Jungfraujoch station
28 The calculated trends for the whole time series showed an increase of 7.34 ± 0.16 %
29 per year (FTIR), 7.12 ± 0.05 % per year (TOMCAT), 7.29 ± 0.16 % per year (ACE) and
30 6.61 ± 0.05 % per year (*in-situ*). The effects of the Kigali Amendment are not yet
31 visible, as it only came into force in 2019. The seasonal cycle of HFC-134a over the
32 Jungfraujoch showed a maximum atmospheric load at the end of summer and a
33 minimum at the end of spring, which could be driven by the tropopause height.

34 As reported in the Scientific Assessment of Ozone Depletion (2022) [5], global
35 top-down derived emissions of HFCs show a significant gap with the total HFC
36 emissions reported by Annex I countries to the UNFCCC in 2019. Understanding these
37 differences between the reported and estimated emissions requires continuous
38 atmospheric monitoring in support to the Kigali Amendment. The strategy presented
39 in this manuscript has been validated by comparison with three other independent
40 datasets. It could therefore be implemented at other NDACC sites to achieve quasi-
41 global coverage of this species using the FTIR remote sensing technique.

1 **Authors contribution**

2 IPC: conceptualization, data curation, formal analysis, investigation, methodology,
3 software, visualization, writing - original draft.

4 EM: conceptualization, data curation, funding acquisition, investigation,
5 methodology, project administration, supervision, and writing - review & editing.

6 MPC: data curation, validation, resources, and writing - review & editing.

7 CS: spectra acquisition, instrumental maintenance and development.

8 SR: data curation, and writing - review & editing.

9 MKV: *in-situ* measurements, data curation, and writing - review & editing.

10

11 **Declaration of Competing Interest**

12 Authors of this manuscript have no competing interests to declare.

13

14 **Research data**

15 The Jungfraujoch FTIR data are available upon request (i.pardocantos@uliege.be).

16 The *in-situ* Jungfraujoch data are available at the AGAGE website
17 (https://agage2.eas.gatech.edu/data_archive/agage/). ACE-FTS data are available at
18 the ACE/SCISAT Database (<https://databace.scisat.ca/level2/>).

19

20 **Acknowledgements**

21 This work was supported by the Fonds de la Recherche Scientifique (F.R.S. – FNRS,
22 Brussels, Belgium) [grant no. J.0126.21], the GAW-CH program of MeteoSwiss
23 (Zürich, CH) and the University of Liège (Belgium). EM is a senior research associate
24 with F.R.S. – FNRS. The ULiège team thanks the International Foundation High
25 Altitude Research Stations Jungfraujoch and Gornergrat (HFSJG, Bern, CH) for
26 supporting the facilities needed to perform the Fourier Transform InfraRed
27 observations at Jungfraujoch. MPC was supported by the UK Natural Environment
28 Research Council SISLAC (NE/R001782/1) and LSO3 (NE/V011863/1) projects. The
29 TOMCAT model runs were performed on the UK Archer and University of Leeds ARC
30 computers. We thank Wuhu Feng (NCAS) for help with the ECMWF meteorology. The
31 AGAGE operation at Jungfraujoch is funded by the Swiss National Programs
32 HALCLIM and CLIMGAS-CH (Swiss Federal Office for the Environment, FOEN), by
33 the international Foundation for High Altitude Research Stations Jungfraujoch and
34 Gornergrat (HFSJG). We thank Dr G. C. Toon for developing, maintaining and making
35 available the pseudo-line lists (PLLs) and the ATM20 spectroscopic compilation that
36 were essential to the present work. The Atmospheric Chemistry Experiment (ACE) is
37 funded by the Canadian Space Agency and we thank the whole team for the ACE-
38 FTS retrievals of HFC-134a.

39

40 **Supplementary materials**

41 Supplementary material associated with this article can be found, in the online version,
42 at doi: 10.1016/j.jqsrt.2024.108938.

1 **References**

- 2 [1] Molina, M. J. and Rowland, F. S. (1974) Stratospheric sink for
3 chlorofluoromethanes: chlorine atom-catalysed destruction of ozone, *Nature*, 249,
4 810-812, DOI: 10.1038/249810a0.
- 5
- 6 [2] Harrison, J. J., Chipperfield, M. P., Boone, C. D., Dhomse, S. S., and Bernath, P.
7 F. (2021). Fifteen years of HFC-134a satellite observations: Comparisons with
8 SLIMCAT calculations. *Journal of Geophysical Research: Atmospheres*, 126,
9 e2020JD033208. DOI: 10.1029/2020JD033208.
- 10
- 11 [3] Velders, G. J., Daniel, J. S., Montzka, S. A., Vimont, I., Rigby, M., Krummel, P. B.,
12 Muhle, J., O'Doherty, S., Prinn, R. G., Weiss, R. F. and Young, D. (2022). Projections
13 of hydrofluorocarbon (HFC) emissions and the resulting global warming based on
14 recent trends in observed abundances and current policies. *Atmospheric Chemistry*
15 *and Physics*, 22(9), 6087-6101. DOI: 10.5194/acp-22-6087-2022.
- 16
- 17 [4] Liang, Q., Rigby, M. et al., Chapter 2: Hydrofluorocarbons (HFCs). World
18 Meteorological Organization (WMO). *Scientific Assessment of Ozone Depletion: 2022*,
19 Ozone Research and Monitoring, GAW Report No. 278, 509 pp.; WMO: Geneva,
20 2022.
- 21
- 22 [5] World Meteorological Organization (WMO). *Scientific Assessment of Ozone*
23 *Depletion: 2022*, Ozone Research and Monitoring, GAW Report No. 278, 509 pp.;
24 WMO: Geneva, 2022.
- 25
- 26 [6] Burkholder, J. B., Hodnebrog, O. et al., Annex: Summary of Abundances, Lifetimes,
27 ODPs, REs, GWPs, and GTPs. World Meteorological Organization (WMO). *Scientific*
28 *Assessment of Ozone Depletion: 2022*, Ozone Research and Monitoring, GAW Report
29 No. 278, 509 pp.; WMO: Geneva, 2022.
- 30
- 31 [7] Daniel, J. S., Reimann, S. et al., Chapter 7: Scenarios and Information for
32 Policymakers. World Meteorological Organization (WMO). *Scientific Assessment of*
33 *Ozone Depletion: 2022*, Ozone Research and Monitoring, GAW Report No. 278, 509
34 pp.; WMO: Geneva, 2022.
- 35
- 36 [8] Montzka, S. A., Myers, R. C., Butler, J. H., Elkins, J. W., Lock, L. T., Clarke, A. D.,
37 and Goldstein, A. H. (1996). Observations of HFC-134a in the remote
38 troposphere. *Geophysical research letters*, 23(2), 169-172. DOI: 10.1029/95GL03590
- 39
- 40 [9] Montzka, S. A., McFarland, M., Andersen, S. O., Miller, B. R., Fahey, D. W., Hall,
41 B. D., Hu, L., Siso, C. and Elkins, J. W. (2015). Recent trends in global emissions of
42 hydrochlorofluorocarbons and hydrofluorocarbons: Reflecting on the 2007
43 adjustments to the Montreal Protocol. *The Journal of Physical Chemistry A*, 119(19),
44 4439-4449. DOI: 10.1021/jp5097376.
- 45
- 46 [10] Mahieu, E., Fischer, E. V., Franco, B., Palm, M., Wizenberg, T., Smale, D.,
47 Clarisse, L., Clerbaux, C., Coheur, P.F., Hannigan, J. W., Lutsch, E., Notholt, J., Pardo
48 Cantos, I., Prignon, M., Servais, C. and Strong, K. (2021). First retrievals of
49 peroxyacetyl nitrate (PAN) from ground-based FTIR solar spectra recorded at remote

- 1 sites, comparison with model and satellite data. *Elem Sci Anth*, 9(1), 00027. DOI:
2 10.1525/elementa.2021.00027.
3
- 4 [11] Zander, R., Mahieu, E., Demoulin, P., Duchatelet, P., Roland, G., Servais, C., De
5 Mazière, M., Reimann, S., Rinsland, C.P. (2008). Our changing atmosphere: Evidence
6 based on long-term infrared solar observations at the Jungfrauoch since 1950.
7 *Science of The Total Environment* 391(2–3): 184–195. DOI:
8 10.1016/j.scitotenv.2007.10.018.
9
- 10 [12] De Mazière, M., Thompson, A. M., Kurylo, M. J., Wild, J. D., Bernhard, G.,
11 Blumenstock, T., Braathen, G. O., Hannigan, J. W., Lambert, J.-C., Leblanc, T.,
12 McGee, T. J., Nedoluha, G., Petropavlovskikh, I., Seckmeyer, G., Simon, P.C.,
13 Steinbrecht, W. and Strahan, S. E. (2018) The Network for the Detection of
14 Atmospheric Composition Change (NDACC): history, status and perspectives,
15 *Atmospheric Chemistry and Physics*, 18(7), 4935–4964, DOI: 10.5194/acp-18-4935-
16 2018.
17
- 18 [13] Reimann, S., Vollmer, M. K., Hill, M., Schläuri, P., Guillevic, M., Brunner, D.,
19 Henne, S., Rust, D. and Emmenegger, L. (2020). Long-term observations of
20 atmospheric halogenated organic trace gases. *Chimia*, 74(3), 136-136. DOI:
21 10.2533/chimia.2020.136.
22
- 23 [14] Prinn, R. G., Weiss, R. F., Arduini, J., Arnold, T., DeWitt, H. L., Fraser, P. J., et al.
24 (2018). History of chemically and radiatively important atmospheric gases from the
25 Advanced Global Atmospheric Gases Experiment (AGAGE). *Earth System Science*
26 *Data*, 10(2), 985-1018. DOI: 10.5194/essd-10-985-2018.
27
- 28 [15] Simmonds, P. G., O'Doherty, S., Nickless, G., Sturrock, G. A., Swaby, R., Knight,
29 P., Ricketts, J., Woffendin, G. and Smith, R. (1995). Automated gas
30 chromatograph/mass spectrometer for routine atmospheric field measurements of the
31 CFC replacement compounds, the hydrofluorocarbons and
32 hydrochlorofluorocarbons. *Analytical Chemistry*, 67(4), 717-723. DOI:
33 10.1021/ac00100a005.
34
- 35 [16] Miller, B. R., Weiss, R. F., Salameh, P. K., Tanhua, T., Grealley, B. R., Mühle, J.,
36 and Simmonds, P. G. (2008). Medusa: A sample preconcentration and GC/MS
37 detector system for in situ measurements of atmospheric trace halocarbons,
38 hydrocarbons, and sulfur compounds. *Analytical Chemistry*, 80(5), 1536-1545. DOI:
39 10.1021/ac702084k.
40
- 41 [17] O'Doherty, S., Simmonds, P. G., Cunnold, D. M., Wang, H. J., Sturrock, G. A.,
42 Fraser, P. J., Ryall, D., Derwent, R. G., Weiss, R. F., Salameh, P., Miller, B. R., and
43 Prinn, R. G. (2001). In situ chloroform measurements at Advanced Global Atmospheric
44 Gases Experiment atmospheric research stations from 1994 to 1998. *Journal of*
45 *Geophysical Research: Atmospheres*, 106(D17), 20429-20444. DOI:
46 10.1029/2000JD900792.
47
- 48 [18] Cunnold, D. M., Steele, L. P., Fraser, P. J., Simmonds, P. G., Prinn, R. G., Weiss,
49 R. F., Porter, L. W., O'Doherty, S., Langenfelds, R. L., Krummel, P. B., Wang, H. J.,

- 1 Emmons, L., Tie, X. X., and Dlugokencky, E. J. (2002). In situ measurements of
2 atmospheric methane at GAGE/AGAGE sites during 1985–2000 and resulting source
3 inferences. *Journal of Geophysical Research: Atmospheres*, 107(D14), ACH-20. DOI:
4 10.1029/2001JD001226.
5
- 6 [19] Bernath, P. F., McElroy, C. T., Abrams, M. C., Boone, C. D., Butler, M., Camy-
7 Peyret, C. Carleer, M., Clerbaux, C., Coheur, P.-F., Colin, R., DeCola, P., De Mazière,
8 M., Drummond, J. R., Dufour, D., Evans, W. F. J., Fast, H., Fussen, D., Gilbert, K.,
9 Jennings, D. E., Llewellyn, E. J., Lowe, R. P., Mahieu, E., McConnell, J. C., McHugh,
10 M., McLeod, S. D., Michaud, R., Midwinter, C., Nassar, R., Nichitiu, F., Nowlan, C.,
11 Rinsland, C. P., Rochon, Y. J., Rowlands, N., Semeniuk, K., Simon, P., Skelton, R.,
12 Sloan, J. J., Soucy, M.-A., Strong, K., Tremblay, P., Turnbull, D., Walker, K. A., Walkty,
13 I., Wardle, D. A., Wehrle, V., Zander, R. and Zou, J. (2005). Atmospheric chemistry
14 experiment (ACE): mission overview. *Geophysical research letters*, 32(15). DOI:
15 10.1029/2005GL022386.
16
- 17 [20] Fernando, A. M., Bernath, P. F., and Boone, C. D. (2019). Trends in atmospheric
18 HFC-23 (CHF₃) and HFC-134a abundances. *Journal of Quantitative Spectroscopy
19 and Radiative Transfer*, 238, 106540. DOI: 10.1016/j.jqsrt.2019.06.019.
20
- 21 [21] Boone, C. D., Bernath, P. F., and Lecours, M. (2023). Version 5 Retrievals for
22 ACE-FTS and ACE-Imagers. *Journal of Quantitative Spectroscopy and Radiative
23 Transfer*, 108749. DOI: 10.1016/j.jqsrt.2023.108749.
24
- 25 [22] Chipperfield, M. P. (2006). New version of the TOMCAT/SLIMCAT off-line
26 chemical transport model: Intercomparison of stratospheric tracer
27 experiments. *Quarterly Journal of the Royal Meteorological Society: A journal of the
28 atmospheric sciences, applied meteorology and physical oceanography*, 132(617),
29 1179-1203. DOI:10.1256/qj.05.51, 2006.
30
- 31 [23] Hersbach, H., Bell, B., Berrisford, P., Hirahara, S., Horányi, A., Muñoz-Sabater,
32 J., et al. (2020). The ERA5 global reanalysis. *Quarterly Journal of the Royal
33 Meteorological Society*, 146(730), 1999-2049. DOI: 10.1002/qj.3803.
34
- 35 [24] World Meteorological Organization (WMO). *Scientific Assessment of Ozone
36 Depletion: 2018*, Global Ozone Research and Monitoring Project, GAW Report No.
37 58, 588 pp.; WMO: Geneva, 2018.
38
- 39 [25] Clerbaux, C., Colin, R., Simon, P. C., and Granier, C. (1993). Infrared cross
40 sections and global warming potentials of 10 alternative hydrohalocarbons. *Journal of
41 Geophysical Research: Atmospheres*, 98(D6), 10491-10497. DOI:
42 10.1029/93JD00390.
43
- 44 [26] Highwood, E. J., and Shine, K. P. (2000). Radiative forcing and global warming
45 potentials of 11 halogenated compounds. *Journal of Quantitative Spectroscopy and
46 Radiative Transfer*, 66(2), 169-183. DOI: 10.1016/S0022-4073(99)00215-0.
47
- 48 [27] Nemtchinov, V., and Varanasi, P. (2004). Absorption cross-sections of HFC-134a
49 in the spectral region between 7 and 12 μ m. *Journal of Quantitative Spectroscopy and
50 Radiative Transfer*, 83(3-4), 285-294. DOI: 10.1016/S0022-4073(02)00356-4.

- 1
2 [28] Sharpe, S. W., Johnson, T. J., Sams, R. L., Chu, P. M., Rhoderick, G. C., and
3 Johnson, P. A. (2004). Gas-phase databases for quantitative infrared
4 spectroscopy. *Applied spectroscopy*, 58(12), 1452-1461. DOI:
5 10.1366/0003702042641281.
6
7 [29] Gohar, L. K., Myhre, G., and Shine, K. P. (2004). Updated radiative forcing
8 estimates of four halocarbons. *Journal of Geophysical Research:*
9 *Atmospheres*, 109(D1). DOI: 10.1029/2003JD004320.
10
11 [30] Harrison, J. J. (2015). Infrared absorption cross sections for 1, 1, 1, 2-
12 tetrafluoroethane. *Journal of Quantitative Spectroscopy and Radiative Transfer*, 151,
13 210-216. DOI: 10.1016/j.jqsrt.2014.09.023.
14
15 [31] Rodgers, C. D., *Inverse Methods for Atmospheric Sounding: Theory and Practice*,
16 World Scientific, 2000, vol. 2.
17
18 [32] Gordon, I. E., Rothman, L. S., Hargreaves, R. J., Hashemi, R., Karlovets, E. V.,
19 Skinner, F. M., et al. (2022). The HITRAN2020 molecular spectroscopic
20 database. *Journal of quantitative spectroscopy and radiative transfer*, 277, 107949.
21 DOI: 10.1016/j.jqsrt.2021.107949.
22
23 [33] Gettelman, A., Mills, M. J., Kinnison, D. E., Garcia, R. R., Smith, A. K., Marsh, D.
24 R., Tilmes, S., Vitt, F., Bardeen, C. G., McInerny, J., Liu, H.-L., Solomon, S. C., Polvani,
25 L. M., Emmons, L. K., Lamarque, J.-F., Richter, J. H., Glanville, A. S., Bacmeister, J.
26 T., Phillips, A. S., Neale, R. B., Simpson, I. R., DuVivier, A. K., Hodzic, A. and Randel,
27 W. J. (2019). The Whole Atmosphere Community Climate Model version 6
28 (WACCM6). *Journal of Geophysical Research: Atmospheres*, 124(23), 12380-12403.
29 DOI: 10.1029/2019JD030943.
30
31 [34] Berrisford, P., Dee, D., Poli, P., Brugge, R., Fielding, K., Fuentes, M., et al. (2011).
32 The ERA-Interim archive Version 2.0, Shinfield Park. *Reading*, 1, 23.
33
34 [35] Prignon, M., Chabrillat, S., Minganti, D., O'Doherty, S., Servais, C., Stiller, G.,
35 Toon, G. C., Vollmer, M. K., and Mahieu, E. (2019). Improved FTIR retrieval strategy
36 for HCFC-22 (CHClF₂), comparisons with in situ and satellite datasets with the support
37 of models, and determination of its long-term trend above Jungfraujoch. *Atmospheric*
38 *Chemistry and Physics*, 19(19), 12309-12324. DOI: 10.5194/acp-19-12309-2019.
39
40 [36] Barthlott, S., Schneider, M., Hase, F., Wiese, A., Christner, E., González, Y.,
41 Blumenstock, T., Dohe, S., García, O., Sepúlveda, E., Strong, K., Mendonca, J.,
42 Weaver, D., Palm, M., Deutscher, N. M., Warneke, T., Notholt, J., Lejeune, B., Mahieu,
43 E., Jones, N., Griffith, D. W. T., Velasco, V. A., Smale, D., Robinson, J., Kivi, R.,
44 Heikkinen, P. and Raffalski, U. (2015). Using XCO₂ retrievals for assessing the long-
45 term consistency of NDACC/FTIR data sets. *Atmos. Meas. Tech.*, 8, 1555-1573.
46 DOI:10.5194/amt-8-1555-2015.
47
48 [37] Pardo Cantos, I., Mahieu, E., Chipperfield, M. P., Smale, D., Hannigan, J. W.,
49 Friedrich, M., Fraser, P., Krummel, P., Prignon, M., Makkor, J., Servais, C. and
50 Robinson, J. (2022). Determination and analysis of time series of CFC-11 (CCl₃F) from

1 FTIR solar spectra, in situ observations, and model data in the past 20 years above
2 Jungfrauoch (46° N), Lauder (45° S), and Cape Grim (40° S) stations. *Environmental*
3 *Science: Atmospheres*, 2(6), 1487-1501. DOI: 10.1039/D2EA00060A.

4
5 [38] Sussmann, R., Borsdorff, T., Rettinger, M., Camy-Peyret, C., Demoulin, P.,
6 Duchatelet, P., Mahieu, E., and Servais, C. (2009). Harmonized retrieval of column-
7 integrated atmospheric water vapor from the FTIR network – first examples for long-
8 term records and station trends. *Atmospheric Chemistry and Physics*, 9(22), 8987-
9 8999. DOI: 10.5194/acp-9-8987-2009.

10
11 [39] Friedrich, M., Smeekes, S., and Urbain, J. P. (2020). Autoregressive wild
12 bootstrap inference for nonparametric trends. *Journal of Econometrics*, 214(1), 81-
13 109. DOI: 10.1016/j.jeconom.2019.05.006.

14
15 [40] Bernath, P. F., Crouse, J., Hughes, R. C., and Boone, C. D. (2021). The
16 Atmospheric Chemistry Experiment Fourier transform spectrometer (ACE-FTS)
17 version 4.1 retrievals: Trends and seasonal distributions. *Journal of Quantitative*
18 *Spectroscopy and Radiative Transfer*, 259, 107409. DOI:
19 10.1016/j.jqsrt.2020.107409.

20
21 [41] Zander, R., Duchatelet, P., Mahieu, E., Demoulin, P., Roland, G., Servais, C.,
22 Auwera, J. V., Perrin, A., Rinsland, C. P., and Crutzen, P. J. (2010). Formic acid above
23 the Jungfrauoch during 1985–2007: observed variability, seasonality, but no long-
24 term background evolution. *Atmospheric Chemistry and Physics*, 10(20), 10047-
25 10065. DOI: 10.5194/acp-10-10047-2010.

26
27 [42] Gardiner, T., Forbes, A., De Mazière, M., Vigouroux, C., Mahieu, E., Demoulin,
28 P., Velazco, V., Notholt, J., Blumenstock, T., Hase, F., Kramer, I., Sussmann, R.,
29 Stremme, W., Mellqvist, J., Strandberg, A., Ellingsen, K., and Gauss, M. (2008). Trend
30 analysis of greenhouse gases over Europe measured by a network of ground-based
31 remote FTIR instruments. *Atmospheric Chemistry and Physics*, 8(22), 6719-6727.
32 DOI: 10.5194/acp-8-6719-2008.